Single Particle Models for the Numerical Simulation of Lithium-ion Cells

Alfredo Ríos Alborés and Jerónimo Rodríguez

Abstract In the design of Battery Management Systems (BMS) for a lithium-ion cell, it is crucial to accurately simulate the device in real-time using mathematical models. Often, Equivalent Circuit Models (ECM) are used to this end, due to their simplicity and efficiency. However, they are purely phenomenological (their parameters are fitted to emulate empirical data) and their internal variables lack physical meaning. On the other hand, the most popular physics-based electrochemical model in the literature, the pseudo-two-dimensional (P2D) model, presents a high computational cost. In this paper, we review the single particle model (SPM), a physics-based model of reduced complexity that is suitable for real-time applications.

1 Introduction

In the last decades, there has been an increasing interest in the development and improvement of electric energy storage devices. The electrochemical batteries based on lithium-ion chemistry present good properties, such as high energy and power density, long life expectancy, low self-discharge rate, non-memory effect, among others [8]. Its advantages, compared to other chemistries, make this technology the preferred candidate for electrical vehicles [14]. However, lithium-ion cells are sensi-

Alfredo Ríos Alborés
Departamento de Matemática Aplicada, Universidade de Santiago de Compostela, 15782 Santiago de Compostela, Spain
ITMATI, Campus Sur, 15706 Santiago de Compostela, Spain
e-mail: alfredo.rios.albores@usc.es

Jerónimo Rodríguez
Departamento de Matemática Aplicada, Universidade de Santiago de Compostela, 15782 Santiago de Compostela, Spain
IMAT, Universidade de Santiago de Compostela, 15706 Santiago de Compostela, Spain
ITMATI, Campus Sur, 15706 Santiago de Compostela, Spain
e-mail: Jeronimo.Rodriguez@usc.es

tive to inappropriate use conditions [3] [4]. Hence, for safety reasons and to improve their performance, it is very important to estimate the cell's state.

For real-time applications, like BMS, a mathematical model is necessary, as a virtual cell. Often, an ECM is implemented [25]. In these models, that are purely phenomenological, their parameters are fitted to reproduce empirical measures. In consequence, the internal variables lack true physical meaning. Modern BMS pretend to implement advanced features, such as optimal/fast charge protocols, cell degradation estimation, and internal cell states monitoring [17] [18]. For such features, physics-based models are better suited than equivalent models.

In the literature, the most popular validated physics-based model is the P2D model, firstly proposed in [9]. From a mathematical point of view, the P2D model can be formulated as a non-linear partial differential equations (PDEs) system, of parabolic and elliptic equations, all of them coupled by non-linear algebraic equations, in particular, Butler-Volmer kinetics equations [12]. Due to its complexity, its computational cost is prohibitive for real-time applications. Different approaches are found in the literature to simplify this model. For example, order reduction techniques [5] [6] [10] [11] or just simplifying assumptions [30] [31]. Among the latter, the SPM is one of the most popular choices. Its formulation is deduced from the P2D model under the main assumption that the intercalation/deintercalation reaction flux across each electrode is homogeneously distributed.

The first examples of SPM considered that the electric potentials and electrolyte physics in the cell are negligible under low C-rate current profiles [22]. In [28], a SPM was compared with a P2D model. The SPM performance was acceptable for low C-rates protocols, up to $1C$. In other works, lithium-ion distribution is modeled in terms of average concentrations in the solid particles, obtaining linear ordinary differential equations, and allowing for a readily implementation of linear filter techniques, such as the Kalman filter [7] [29]. Different approaches have been proposed to enhance the SP model for its use under higher C-rates currents [13] [19] [26]. Furthermore, it can be extended to capture thermal dynamics [2] [23] and to estimate cell degradation over-time [15] [27], using meaningful internal electrochemical quantities of the cells.

In this paper, we review the single particle model with electrolyte dynamics (SPMe) [16] [21]. We focus on its derivation from the P2D model stating and describing the main physical simplifying assumptions. The SPMe is numerically solved using the finite element library FEniCS [1]. The results are compared to those provided by the P2D model in terms of applicability range, accuracy, and computational cost.

Table 1 Nomenclature

Symbol	Units	Name and description
Greek symbols		
$\alpha, 1-\alpha$	1	asymmetric charge transfer coefficients
$\varepsilon_e, \varepsilon_s$	1	volume fraction of the electrolyte and the solid phases
κ	S/m	ionic conductivity of the electrolyte
Ω		macroscale cell domain
$\Omega^-, \Omega^+, \Omega^o$		macroscale subdomains: negative and positive electrode, separator
Ω_{ap}		microscale solid phase domain
ϕ_e, ϕ_s	V	electric potential in the electrolyte and solid phase
$\sigma^{\pm}$	S/m	electric conductivity of the solid phase
θ	K	temperature
Latin symbols		
a_s	m^2/m^3	surface area density of solid particles
brugg	1	Bruggeman coefficient
c_e	mol/m^3	lithium salt concentration in the electrolyte
$c_s^{\pm}$	mol/m^3	intercalated lithium concentration in the solid particles
$c_{s,\max}^{\pm}$	mol/m^3	maximum concentration of intercalated lithium
$D_s^{\pm}, D_e$	m^2/s	solid phase and electrolyte diffusion coefficients
F	C/mol	Faraday's constant
i	A	current intensity
$j_{Li}^{\pm}$	$mol/m^2 s$	lithium intercalation-deintercalation reaction flux at $\Omega^{\pm}$
$k_0^{\pm}$	$\frac{mol^{\frac{-1}{2}}\, m^{\frac{5}{2}}}{s}$	effective rate constant of the in-deintercalation reaction
L^-, L^+, L^o	m	electrodes and separator thickness
L	m	cell thickness, $L := L^- + L^+ + L^o$
r	m	microscale radial space variable
r_{SEI}	m	SEI layer radial thickness
R	$J/K\, mol$	ideal gas constant
R_{col}	Ω	total current collectors resistance
$R_s^{\pm}$	m	average solid particles radius in each electrode
S	m^2	current collectors area
t_+^o	1	ionic transfer number of the electrolyte
$U_{\text{ocp}}^{\pm}$	V	OCP of the positive/negative electrode solid material
V	V	cell voltage
x	m	macroscale space variable
$x_{0\%}, x_{100\%}, y_{0\%}, y_{100\%}$	1	nominal stoichiometry window
$z_{\text{film}}^{\pm}$	Ωm^2	resistance of the film on the solid particles surface

2 The P2D Model

The equations of physics-based models for lithium-ion cells can be naturally deduced applying conservation laws for mass and charge at the three-dimensional particle scale or "micro-scale". Then, using volume-averaging techniques, and under some simplifying assumptions, one can obtain the P2D model equations. Further details and gentle explanations of all this can be found in [24].

For completeness, we state a P2D model equations. We assume that the cell temperature is spatially homogeneous and known at every time, and neglect cell degradation over-time mechanisms. We use a second-order elliptic formulation for

the electric potentials, which is a better-suited formulation for the model resolution using the finite element method. For brevity, we avoid presenting symbols, which are summarized in Table 1.

It is assumed that all the main processes occur in the direction perpendicular to the cell. Therefore, only the cell thickness is accounted as a spatial dimension and the domain of the problem, representing the device, is modeled as an 1D-domain, $\Omega = (0, L)$. Within, we distinguish the negative electrode, the separator and the positive electrode as subdomains, denoted respectively as $\Omega^- = (0, L^-)$, $\Omega^o = (L^-, L^- + L^o)$ and $\Omega^+ = (L^- + L^o, L)$. Furthermore, to model the intercalated lithium diffusion in the solid reactive particles at each electrode, we need to introduce the 2D microscale domain $\Omega_{ap} = \left((0, R_s^-) \times \Omega^-\right) \cup \left((0, R_s^+) \times \Omega^+\right)$. A simple sketch of a cell is represented in Fig. 1. The model equations are stated as follows.

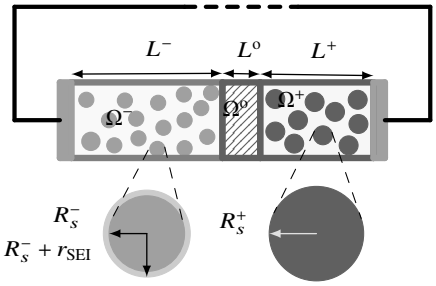

Fig. 1 Sketch of a cell. On the left (resp. right), the negative electrode, Ω^- (resp. positive electrode, Ω^+). In the middle, the separator, Ω^o, which is an electric insulator. At the micro-scale level, the electrode's solid particles are assumed to be spheres. Usually, the SEI layer is formed on the surface of the particles in Ω^-. Modified with permission from [12]

2.1 Butler-Volmer Equation

At every $x \in \Omega^\pm$, the intercalation/deintercalation reaction flux on the solid particle surfaces is modeled using Butler-Volmer kinetics, namely,

$$j_{Li}^\pm(x,t) = \frac{i_0^\pm(x,t)}{F}\left(\exp\left(\frac{(1-\alpha^\pm)F}{R\theta}\eta^\pm(x,t)\right) - \exp\left(-\frac{\alpha^\pm F}{R\theta}\eta^\pm(x,t)\right)\right), \quad (1)$$

where

$$i_0^\pm(x,t) = Fk_0^\pm\left(c_e(x,t)\left(c_{s,\max}^\pm - c_s^\pm\left(R_s^\pm, x, t\right)\right)\right)^{1-\alpha^\pm}\left(c_s^\pm\left(R_s^\pm, x, t\right)\right)^{\alpha^\pm}, \quad (2)$$

$$\eta^{\pm}(x,t) = \phi_s^{\pm}(x,t) - \phi_e(x,t) - U_{\text{ocp}}^{\pm}\left(\frac{c_s^{\pm}\left(R_s^{\pm},x,t\right)}{c_{s,\max}^{\pm}}\right) - Fz_{\text{film}}^{\pm} j_{Li}^{\pm}(x,t). \tag{3}$$

We further define

$$j(x,t) := \begin{cases} j_{Li}^{-}(x,t), & x \in \Omega^{-}, \\ 0, & x \in \Omega^{\text{o}}, \\ j_{Li}^{+}(x,t), & x \in \Omega^{+}. \end{cases} \tag{4}$$

2.2 Intercalated Lithium Concentration in the Solid Particles

The distribution of lithium inside the particles is assumed to respond only to diffusion effects. The corresponding parabolic PDE is defined in the micro-scale 2D-domain, namely,

$$\frac{\partial c_s}{\partial t}(r,x,t) - \frac{1}{r^2}\frac{\partial}{\partial r}\left(D_s r^2 \frac{\partial c_s}{\partial r}(r,x,t)\right) = 0, \text{ in } \Omega_{\text{ap}}, \tag{5}$$

$$\frac{\partial c_s}{\partial r}(0,x,t) = 0, \quad \forall (0,x) \in \Omega_{\text{ap}}, \tag{6}$$

$$-D_s \frac{\partial c_s^{\pm}}{\partial r}\left(R_s^{\pm},x,t\right) = j_{Li}^{\pm}(x,t), \quad \forall \left(R_s^{\pm},x\right) \in \{R_s^{\pm}\} \times \Omega^{\pm}, \tag{7}$$

where $c_s^{\pm}(r,x,t) := c_s(r,x,t)$ in $\left(0,R_s^{\pm}\right) \times \Omega^{\pm}$. Notice that only the boundary condition depends on $x \in \Omega^{\pm}$. Initial conditions, $c_s^{\pm}(r,x,0)$, have to be given.

2.3 Lithium Salt Concentration in the Electrolyte

For the lithium salt distribution in the electrolyte, the model accounts for the diffusion effects, the electroneutrality condition of the medium and the reaction flux as a source term,

$$\frac{\partial(\varepsilon_e c_e)}{\partial t}(x,t) - \frac{\partial}{\partial x}\left(D_e^{\text{eff}}\frac{\partial c_e}{\partial x}(x,t)\right) = \left(1 - t_+^o\right) a_s j(x,t), \text{ in } \Omega, \tag{8}$$

$$\frac{\partial c_e}{\partial x}(0,t) = \frac{\partial c_e}{\partial x}(L,t) = 0, \tag{9}$$

where $D_e^{\text{eff}}(x,t) \equiv D_e(\theta)\,\varepsilon_e(x,t)^{\text{brugg}}$. An initial condition, $c_e(x,0)$, has to be given.

2.4 Electric Potential in the Electrolyte

The electric potential in the electrolyte spatially varies due to the lithium salt gradient effects and due to the electrochemical reaction flux distribution across the cell,

$$\frac{\partial}{\partial x}\left(\kappa^{\text{eff}}\frac{\partial \phi_e}{\partial x}(x,t)\right)+\frac{\partial}{\partial x}\left(\kappa_D^{\text{eff}}\frac{\partial \ln c_e}{\partial x}(x,t)\right)=-Fa_s j(x,t),\ \text{in } \Omega, \tag{10}$$

$$\frac{\partial \phi_e}{\partial x}(0,t)=\frac{\partial \phi_e}{\partial x}(L,t)=0, \tag{11}$$

where $\kappa^{\text{eff}}(x,t)=\kappa(c_e,\theta)\,\varepsilon_e(x)^{\text{brugg}}$, $\kappa_D^{\text{eff}}(x,t)=\kappa_D(x,t)\,\varepsilon_e(x)^{\text{brugg}}$ and $\kappa_D(x,t):=\frac{2\kappa(c_e,\theta)R\theta\left(t_+^o-1\right)}{F}$.

2.5 Electric Potential in the Solid Phase

In the solid phase, the electric potential spatially varies due to the reaction flux distribution across each electrode,

$$\frac{\partial}{\partial x}\left(-\sigma^{\text{eff}}\frac{\partial \phi_s}{\partial x}(x,t)\right)=-Fa_s j(x,t),\ \text{in } \Omega^-\cup\Omega^+, \tag{12}$$

$$\frac{\partial \phi_s^-}{\partial x}(L^-,t)=\frac{\partial \phi_s^+}{\partial x}(L^-+L^{\text{o}},t)=0, \tag{13}$$

$$-\sigma^{\text{eff}}\frac{\partial \phi_s^-}{\partial x}(0,t)=-\sigma^{\text{eff}}\frac{\partial \phi_s^+}{\partial x}(L,t)=\frac{i(t)}{S}, \tag{14}$$

where $\sigma^{\text{eff}}(x,t)=\sigma(\theta)\,\varepsilon_s(x)^{\text{brugg}}$. We are assuming that the current signal, $i(t)$, is given, so that the PDE is stated using Neumann boundary conditions.

2.6 Gauge Conditions on Potentials

Notice that we cannot expect uniqueness of solution for this model. Indeed, disregarding the Butler-Volmer equation, both potentials are always affected by a derivative. Moreover, the dependence on the potentials in the Butler-Volmer equation is through the difference $\phi_s(x,t)-\phi_e(x,t)$. In consequence, if we find a solution to the system, by adding a constant to both potentials (the same for both), we would get a different new solution. For that reason, it is necessary to impose a gauge condition only on one of them. In this study, we propose the condition

$$\int_\Omega \phi_e(x,t)\ \mathrm{d}x=0. \tag{15}$$

3 Derivation of the SPM

We will now derive the SPM from the P2D equations presented in the previous section. A similar derivation process has been addressed in [21].

We consider that, initially, the cell is in rest and in steady-state. Hence, the spatial distribution of intercalated lithium in the solid phase at each electrode is approximately homogeneous, $c_s^{\pm}(r,x,0) = c_{s,0}^{\pm}$, with $c_{s,0}^{\pm} \in \mathbb{R}^+$. And the same is true for the lithium salt in the electrolyte across the entire cell, $c_e(x,0) = c_{e,0}$, with $c_{e,0} \in \mathbb{R}^+$. Then, we assume:

- A_1 Some cell material properties are constant per subdomain. In particular: $\varepsilon_e(x)$, $\varepsilon_s(x)$, $R_s(x)$ and $\kappa(c_e,\theta)$.
- A_2 The electrochemical reaction flux distribution of the intercalation/deintercalation process is homogeneous across each electrode. Namely, $j_{Li}^{\pm}(x,t) \equiv j_{Li}^{\pm}(t)$, in $\Omega^{\pm}$.
- A_2 $\alpha^{\pm} = (1-\alpha^{\pm}) \equiv \alpha = 1/2$.

Remark 1 Assumption A_3 is not strictly necessary to derive a single-particle model. Nevertheless, it simplifies the resolution of the model (see *Remark* 2). In the literature, A_3 is assumed frequently, even when dealing with the P2D model.

Next, we apply assumptions A_1 - A_3 to the P2D model (1 - 15). We will refer to figures of numerical result to illustrate qualitative properties of the new model equations, even though the technical details of those numerical experiments will not be given until the next section.

3.1 Butler-Volmer Equation

Now, (1 - 3) become

$$j_{Li}^{\pm}(t) = \frac{1}{F} i_{0,\text{avg}}^{\pm}(t) \left(\exp\left(\frac{\alpha F}{R\theta} \eta^{\pm}(t) \right) - \exp\left(-\frac{\alpha F}{R\theta} \eta^{\pm}(t) \right) \right), \text{ in } \Omega^{\pm}, \tag{16}$$

$$i_{0,\text{avg}}^{\pm}(t) := \frac{1}{L^{\pm}} \int_{\Omega^{\pm}} F k_0^{\pm} \left(\left(c_{s,\max}^{\pm} - c_s^{\pm}\left(R_s^{\pm},t\right) \right) c_e(x,t)\, c_s^{\pm}\left(R_s^{\pm},t\right) \right)^{\alpha} \, \mathrm{d}x, \tag{17}$$

$$\eta^{\pm}(t) = \phi_s^{\pm}(x,t) - \phi_e^{\pm}(x,t) - U_{\text{ocp}}^{\pm}\left(c_s^{\pm}\left(R_s^{\pm},t\right)\right) - F z_{\text{film}}^{\pm} j_{Li}^{\pm}(t). \tag{18}$$

In each electrode, we have approximated the exchange current density $i_0^{\pm}(x,t)$ in (2) by its average, $i_{0,\text{avg}}^{\pm}(t)$, and assumed that the overpotential $\eta^{\pm}(x,t) \approx \eta^{\pm}(t)$. In practice, $k_0^{\pm}$ is usually given as a constant value per electrode. In that case, to compute $i_{0,\text{avg}}^{\pm}(t)$, it would be enough to average the lithium salt distribution function

$c_e(x,t)^{\alpha}$ in $\Omega^{\pm}$. Notice that, to all this to be physically accurate, $c_e(x,t)$ and the difference $\phi_s(x,t) - \phi_e(x,t)$ have to be *homogeneous enough* across the electrodes.

Integrating (12) across each electrode, applying boundary conditions (13-14), we obtain an explicit linear expression for $j(x,t)$ as a linear function of the current,

$$j(x,t) = \begin{cases} j_{Li}^{-}(t) = \frac{i(t)}{FSL^{-}a_s^{-}}, \text{ in } \Omega^{-}, \\ 0, \text{ in } \Omega^{\text{o}}, \\ j_{Li}^{+}(t) = -\frac{i(t)}{FSL^{+}a_s^{+}}, \quad \text{in } \Omega^{+}. \end{cases} \tag{19}$$

Furthermore, (16) is analytically invertible, and its left-hand side is given by (19). Then,

$$\eta^{\pm}(t) = \frac{R\theta}{\alpha F}\sinh^{-1}\left(\frac{j_{Li}^{\pm}(t)\,F}{2i_{0,\text{avg}}^{\pm}(t)}\right) = \frac{R\theta}{\alpha F}\sinh^{-1}\left(\mp\frac{i(t)}{2i_{0,\text{avg}}^{\pm}(t)\,SL^{\pm}a_s^{\pm}}\right). \tag{20}$$

Remark 2 Notice that we have used A_3 to obtain this closed form for $\eta^{\pm}(t)$. The values of coefficients $\alpha^{\pm}$ could be, eventually, different. This would require solving (16) as non-linear equations.

3.2 Intercalated Lithium Concentration in the Solid Particles

The PDE (5 - 7) is no longer x-dependent, because $j_{Li}^{\pm}(t)$ is homogeneous across $\Omega^{\pm}$. Moreover, we are assuming that $\varepsilon_s(x)$ and $R_s(x)$ are constant per subdomain (A_1), i.e., that the distribution and size of the solid particles are homogeneous and constant across each electrode. As a consequence, every solid particle in $\Omega^{\pm}$ will behave the same and, then, $c_s^{\pm}(r,x,t) \equiv c_s^{\pm}(r,t)$. It will be enough to solve the following two linear parabolic PDEs,

$$\frac{\partial c_s^{\pm}}{\partial t}(r,t) - \frac{1}{r^2}\frac{\partial}{\partial r}\left(D_s r^2 \frac{\partial c_s^{\pm}}{\partial r}(r,t)\right) = 0, \quad r \in \left(0, R_s^{\pm}\right), \tag{21}$$

$$\frac{\partial c_s^{\pm}}{\partial r}(0,t) = 0, \tag{22}$$

$$-D_s\frac{\partial c_s^{\pm}}{\partial r}\left(R_s^{\pm},t\right) = \mp\frac{i(t)}{FSL^{\pm}a_s^{\pm}}. \tag{23}$$

Notice that the two-dimensional micro-scale domain of the P2D model has been simplified to a one-dimensional domain. In each electrode, the intercalated lithium distribution profile of the single particle, modeled by (21 - 23), will be an average of the heterogeneous distribution of solid particles across the electrode in the P2D model, as it is shown in Fig. 2 and Fig. 3.

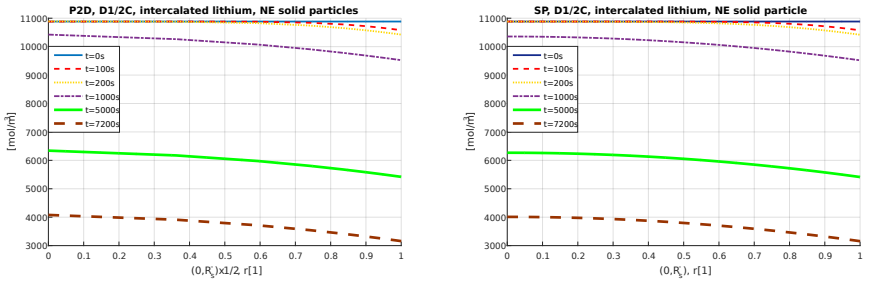

Fig. 2 Discharge under constant $0.5C$-rate. Lithium distribution within particles of the negative electrode, at the middle of the electrode ($x = 1/2$) for the P2D model (left), and for the SP model (right)

3.3 Lithium Salt Concentration in the Electrolyte

Under assumptions A_1 and A_2, the coefficients of (8) become constant per subdomain, and the source term is given by (19). Thus, the equation becomes a linear parabolic PDE, uncoupled from the rest of the equations of the model. Compared to the P2D model, the biggest differences should appear when this source term is far from being spatially homogeneous. For current signals that are piece-wise constant over time, that is especially true the first moments after a change in the current magnitude. When the current signal stays constant, both models reach, eventually, similar steady-state profiles. This is illustrated in Fig. 4 and Fig. 5.

3.4 Cell Voltage

In the P2D model, the cell voltage is typically computed as

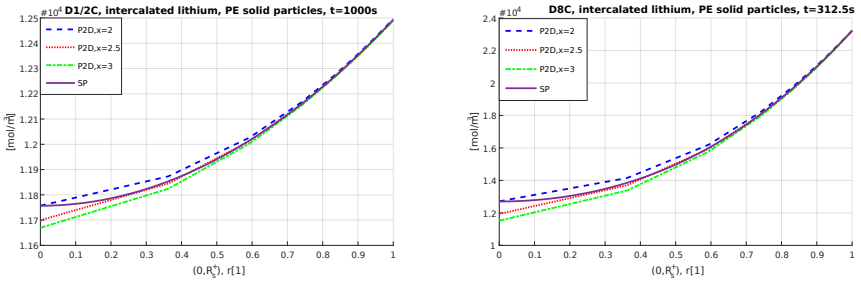

Fig. 3 Discharge under constant $0.5C$-rate (left) and $8C$-rate (right). Lithium concentration distribution inside the solid particles of the positive electrode. For the P2D model, we are representing values inside the particles at the end sides and at the middle of the electrode

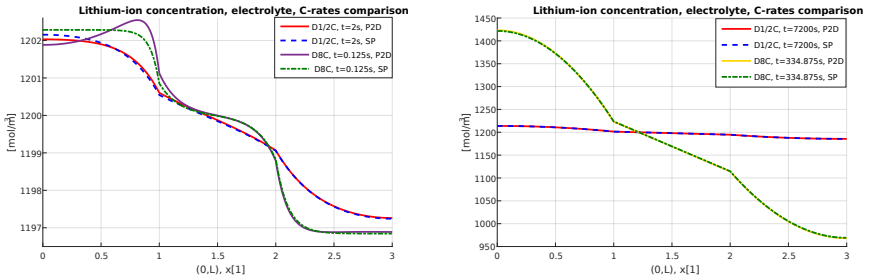

Fig. 4 Discharge under constant 0.5 and 8C-rates. Lithium salt concentration in the electrolyte at the first (left) and the last (right) time step simulated

$$V(t) = \phi_s^+(L,t) - \phi_s^-(0,t) - R_{\text{col}} i(t). \tag{24}$$

For our SPM, we can use (18) and (20) to obtain an explicit expression of voltage as a non-linear function of current and lithium concentration in the different phases. Hence, it is not necessary to solve PDEs (10 - 15). Indeed, from (18),

$$\phi_s^+(L,t) - \phi_s^-(0,t) = \phi_e(L,t) - \phi_e(0,t) - \left(\frac{z^+_{\text{film}}}{L^+ a_s^+} + \frac{z^-_{\text{film}}}{L^- a_s^-}\right)\frac{i(t)}{S} + \eta^+(t) \tag{25}$$

$$-\eta^-(t) + U^+_{\text{ocp}}\left(\frac{c_s^+(R_s^+,t)}{c^+_{s,\max}}\right) - U^-_{\text{ocp}}\left(\frac{c_s^-(R_s^-,t)}{c^-_{s,\max}}\right). \tag{26}$$

We recall the assumption that κ^{eff} and κ_D^{eff} are constant per subdomain (A_1). Integrating (10) across Ω, one can deduce the equality

$$\phi_e(L,t) \; - \; \phi_e(0,t) = -\frac{2R\theta}{F}\left(t_+^o - 1\right)\left(\ln\left(c_e(L,t)\right) - \ln\left(c_e(0,t)\right)\right) \tag{27}$$

$$-\frac{i(t)}{2S}\left(\frac{L^-}{\kappa^{\text{eff},-}} + \frac{2L^{\text{o}}}{\kappa^{\text{eff,o}}} + \frac{L^+}{\kappa^{\text{eff},+}}\right). \tag{28}$$

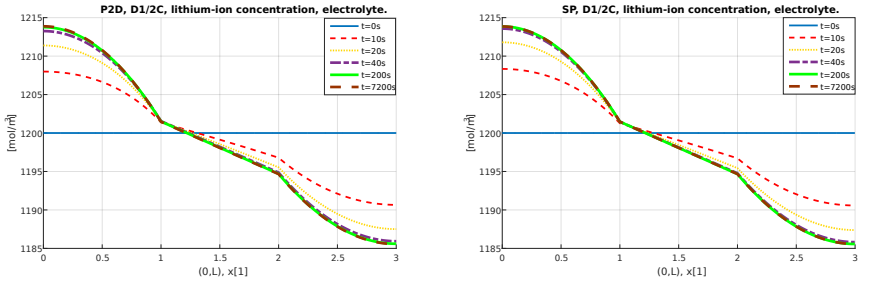

Fig. 5 Discharge under constant 0.5C-rate. Lithium salt distribution across the cell for the P2D (left) and SP (right) models, at different times

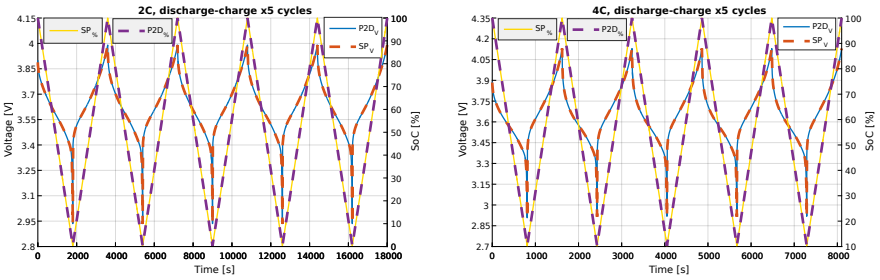

Fig. 6 Cell voltage and state of charge values obtained using the P2D and SP models for 5 discharge-charge cycles, under constant C-rate current signals

Substituting (20), (25 - 26) and (27 - 28) in (24), we finally obtain

$$V(t) = \frac{R\theta}{\alpha F}\left(\sinh^{-1}\left(-\frac{i(t)}{2Sa_s^+ i_{0,\mathrm{avg}}^+(t)L^+}\right) - \sinh^{-1}\left(\frac{i(t)}{2Sa_s^- i_{0,\mathrm{avg}}^-(t)L^-}\right)\right) \tag{29}$$

$$-\left(\frac{z_{\mathrm{film}}^+}{L^+a_s^+} + \frac{z_{\mathrm{film}}^-}{L^-a_s^-}\right)\frac{i(t)}{S} - \left(\frac{L^-}{\kappa^{\mathrm{eff},-}} + \frac{2L^{\mathrm{o}}}{\kappa^{\mathrm{eff,o}}} + \frac{L^+}{\kappa^{\mathrm{eff},+}}\right)\frac{i(t)}{2S} \tag{30}$$

$$-R_{\mathrm{col}}i(t) - \frac{2R\theta}{F}\left(t_+^o - 1\right)\left(\ln\left(c_e(L,t)\right) - \ln\left(c_e(0,t)\right)\right) \tag{31}$$

$$+U_{\mathrm{ocp}}^+\left(\frac{c_s^+\left(R_s^+,t\right)}{c_{s,\max}^+}\right) - U_{\mathrm{ocp}}^-\left(\frac{c_s^-\left(R_s^-,t\right)}{c_{s,\max}^-}\right). \tag{32}$$

The SPM expression for the cell voltage accounts for solid particles saturation at their surfaces, the lithium salt gradient in the electrolyte, and materials resistance effects. We find a good agreement between the qualitative behavior of cell voltage computed with the P2D and the SPM, both capturing cell polarization and relaxation effects under high C-rates, Fig. 6 and Fig. 7.

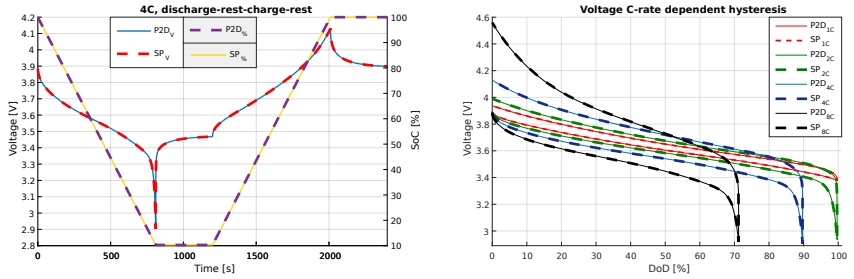

Fig. 7 Cell voltage phenomenology captured by both P2D and SP models. To the left, relaxation effects. To the right, under constant current discharges-charges, voltage *C-rate dependent hysteresis* as a function of the cell deep of discharge, due to the difference between average and surface lithium saturation of solid particles

3.5 State of Charge of the Cell

The state of charge (SoC) of a cell is a measure of the amount of charge stored in the device.

In physics-based models, it can be expressed in terms of the average lithium saturation of the solid phase, in any of the electrodes. Using the SPM, the average lithium concentration of intercalated lithium in each electrode can be computed as

$$c^{\pm}_{s,\mathrm{avg}}(t) \;=\; \frac{3}{R_s^{\pm 3}} \int_0^{R_s^{\pm}} r^2 c_s^{\pm}(r,t)\; \mathrm{d}r. \tag{33}$$

Then, we relatively measure the state of charge of the cell, with respect to the nominal stoichiometry coefficients, as a linear function of $c^{\pm}_{s,\mathrm{avg}}(t)$ by the expression

$$\frac{\mathrm{SoC}(t)}{100} = \frac{\frac{c^{-}_{s,\mathrm{avg}}(t)}{c^{-}_{s,\max}} - x_{0\%}}{x_{100\%} - x_{0\%}} = 1 - \frac{\frac{c^{+}_{s,\mathrm{avg}}(t)}{c^{+}_{s,\max}} - y_{0\%}}{y_{100\%} - y_{0\%}}. \tag{34}$$

The presented models in this work (P2D model and SPM) conserve charge and mass in terms of the current signal. Hence, SoC is equivalently estimated for both, since the SPM just averages the P2D dynamics.

4 Numerical Results

In the previous section, we have discussed some qualitative properties of the SPM using numerical results. We give now the technical and quantitative details of the numerical experiments. We did not aim for an optimal choice of meshes or implementation of the SPM in terms of computational cost and accuracy. The experiments were designed to get an insightful first approach to the SPM features. Every result presented could be potentially improved. Our main goal was to summarize the SPM performance, comparing it with the original P2D model.

The P2D equations present several implementation challenges: different spatial scales domains, non-linear coupled parabolic and elliptic PDEs, non-linear algebraic constraints (Butler-Volmer kinetics), etc. Numerical simulations of this model have been carried out using a *Repsol*[1] & *Itmati*[2] software, temporally ceded for this work [12].

On the other hand, the SPM derived consists of three decoupled, one-dimensional and linear parabolic PDEs. The cell voltage is expressed as a non-linear function of

[1] www.repsol.com

[2] www.itmati.com

the current and the lithium concentrations value in the different phases. When simulating for a given current signal, one can compute the cell voltage as a post-process, after the numerical resolution of the model. Due to its linearity and simplicity, it presents a classical variational formulation for parabolic PDEs, using weighted Sobolev functional spaces in the case of spherical PDEs. For its numerical resolution, the finite element method library FEniCS [1] with linear Lagrange elements has been used.

Several charge and discharge protocols with piece-wise constant current signals were considered. For both models, an implicit Euler integrator was used, with a fixed time discretization step, computed as $dt = \frac{1}{n}[s]$, whenever the current applied as input was a nC-rate signal, with $n \in \mathbb{N}$. The parameters data of the cell models were taken from [20]. Models were run in a laptop computer with processor *Intel(R) Core(TM) i5-6200U CPU @ 2.30 GHz 2.40 GHz* with 8GB RAM memory and 64-bits Windows 10 (OS).

Notice that the SPM does not present a two-dimensional micro-scale domain, as the P2D model does. Therefore, the number of degrees of freedom of the discretized problem is greatly reduced, as shown in Table 2, where we summarize the number of nodes of the meshes involved in the computations. The simplicity of the SPM allows avoiding several not negligible technical difficulties of the P2D model numerical resolution like, for example, the micro-macro scale coupling.

In Table 3 we compare voltage value difference between models and computational times for single discharges under constant C-rate current signals. As expected, the voltage differences norm grows for higher C-rates. But, the relative maximum difference is similar for every current signal. Notice that the greatest differences occur at the beginning of the discharge simulations when P2D dynamics are far from being homogeneous at each electrode. The SPM does not capture the reaction flux behavior for those instants, under any C-rate current signal.

Table 2 Mesh data for each model

Subdomain	Dimension	Number of nodes
P2D model		
Ω	1D	300
$\Omega^{\pm}$	1D	100
$(0, R_s^{\pm}) \times \Omega^{\pm}$	2D	10000
SPM		
Ω	1D	100
$(0, R_s^{\pm})$	1D	100

Table 3 Voltage values and computational times comparison between the P2D and the SP models, under different constant C-rate discharges

	0.5C	1C	2C	4C	8C
Voltage					
Max. error	2.889%	2.887%	2.885%	2.882%	2.877%
$\|\boldsymbol{V}^h_{\text{P2D}} - \boldsymbol{V}^h_{\text{SPe}}\|_2$	0.0063	0.0123	0.0441	0.0524	0.08598
Resolution time					
SPe	97.9s	108.0s	121.8s	100.9s	74.0s
P2D	3246s	3470s	3320s	3279s	2700s
Gain	×33	×32	×27	×32	×36

5 Conclusions

Assuming homogeneous and known cell temperature, and neglecting degradation mechanisms over-time, a single particle model with electrolyte dynamics has been deduced from a P2D model. We have stated the necessary simplifying assumptions for the model derivation and exemplified their consequences with numerical experiments.

The SPM presents a linear formulation of uncoupled one-dimensional parabolic PDEs and, hence, its implementation is straightforward. Compared to the P2D model, the number of degrees of freedom of the discretized problem can be significantly reduced, while obtaining equivalent estimations of the cell state of charge, and a good agreement for the voltage estimation under high C-rate constant current protocols. With a maximum of, approximately, 3% difference in voltage estimation, the computational cost was reduced up to 27-36 times. All this justifies the SPM potential as a physics-based model of reduced complexity for real-time applications.

Acknowledgments

Under the academic supervision of Dr. Jerónimo Rodríguez García, this work was carried out as a Master's thesis for the *Máster en matemática industrial*[3] program offered by *Universidade de Santiago de Compostela*. The project was proposed by *Itmati*, with *Repsol* collaboration, who temporally ceded software to obtain some of the numerical results presented.

[3] www.m2i.es

References

[1] Alnæs, M., Blechta, J., Hake, J., Johansson, A., Kehlet, B., Logg, A., Richardson, C., Ring, J., Rognes, M.E., Wells, G.N.: The fenics project version 1.5. Archive of Numerical Software **3**(100) (2015)

[2] Baba, N., Yoshida, H., Nagaoka, M., Okuda, C., Kawauchi, S.: Numerical simulation of thermal behavior of lithium-ion secondary batteries using the enhanced single particle model. Journal of Power Sources **252**, 214–228 (2014)

[3] Balakrishnan, P., Ramesh, R., Kumar, T.P.: Safety mechanisms in lithium-ion batteries. Journal of Power Sources **155**(2), 401–414 (2006)

[4] Biensan, P., Simon, B., Peres, J., De Guibert, A., Broussely, M., Bodet, J., Perton, F.: On safety of lithium-ion cells. Journal of Power Sources **81**, 906–912 (1999)

[5] Cai, L., White, R.E.: Reduction of model order based on proper orthogonal decomposition for lithium-ion battery simulations. Journal of The Electrochemical Society **156**(3), A154–A161 (2009)

[6] Chu, Z., Plett, G.L., Trimboli, M.S., Ouyang, M.: A control-oriented electrochemical model for lithium-ion battery, part i: Lumped-parameter reduced-order model with constant phase element. Journal of Energy Storage **25**, 100828 (2019)

[7] Di Domenico, D., Stefanopoulou, A., Fiengo, G.: Lithium-ion battery state of charge and critical surface charge estimation using an electrochemical model-based extended kalman filter. Journal of dynamic systems, measurement, and control **132**(6), 061302 (2010)

[8] Diouf, B., Pode, R.: Potential of lithium-ion batteries in renewable energy. Renewable Energy **76**, 375–380 (2015)

[9] Doyle, M., Fuller, T.F., Newman, J.: Modeling of galvanostatic charge and discharge of the lithium/polymer/insertion cell. Journal of the Electrochemical society **140**(6), 1526–1533 (1993)

[10] Fan, G., Li, X., Canova, M.: A reduced-order electrochemical model of li-ion batteries for control and estimation applications. IEEE Transactions on Vehicular Technology **67**(1), 76–91 (2017)

[11] Forman, J.C., Bashash, S., Stein, J.L., Fathy, H.K.: Reduction of an electrochemistry-based li-ion battery model via quasi-linearization and pade approximation. Journal of the Electrochemical Society **158**(2), A93–A101 (2011)

[12] Giráldez, D.A., Cao-Rial, M.T., Muiños, P.F., Rodríguez, J.: Numerical simulation of a li-ion cell using a thermoelectrochemical model including degradation. In: European Consortium for Mathematics in Industry, pp. 535–543. Springer (2016)

[13] Han, X., Ouyang, M., Lu, L., Li, J.: Simplification of physics-based electrochemical model for lithium ion battery on electric vehicle. part i: Diffusion simplification and single particle model. Journal of Power Sources **278**, 802–813 (2015)

[14] Kennedy, B., Patterson, D., Camilleri, S.: Use of lithium-ion batteries in electric vehicles. Journal of Power Sources **90**(2), 156–162 (2000)
[15] Li, J., Adewuyi, K., Lotfi, N., Landers, R.G., Park, J.: A single particle model with chemical/mechanical degradation physics for lithium ion battery state of health (soh) estimation. Applied energy **212**, 1178–1190 (2018)
[16] Li, J., Lotfi, N., Landers, R.G., Park, J.: A single particle model for lithium-ion batteries with electrolyte and stress-enhanced diffusion physics. Journal of The Electrochemical Society **164**(4), A874–A883 (2017)
[17] Lin, X., Kim, Y., Mohan, S., Siegel, J.B., Stefanopoulou, A.G.: Modeling and estimation for advanced battery management. Annual Review of Control, Robotics, and Autonomous Systems **2**, 393–426 (2019)
[18] Lu, L., Han, X., Li, J., Hua, J., Ouyang, M.: A review on the key issues for lithium-ion battery management in electric vehicles. Journal of power sources **226**, 272–288 (2013)
[19] Luo, W., Lyu, C., Wang, L., Zhang, L.: A new extension of physics-based single particle model for higher charge–discharge rates. Journal of Power Sources **241**, 295–310 (2013)
[20] Mazumder, S., Lu, J.: Faster-than-real-time simulation of lithium ion batteries with full spatial and temporal resolution. International Journal of Electrochemistry **2013** (2013)
[21] Moura, S.J., Argomedo, F.B., Klein, R., Mirtabatabaei, A., Krstic, M.: Battery state estimation for a single particle model with electrolyte dynamics. IEEE Transactions on Control Systems Technology **25**(2), 453–468 (2016)
[22] Ning, G., Popov, B.N.: Cycle life modeling of lithium-ion batteries. Journal of The Electrochemical Society **151**(10), A1584–A1591 (2004)
[23] Perez, H., Dey, S., Hu, X., Moura, S.: Optimal charging of li-ion batteries via a single particle model with electrolyte and thermal dynamics. Journal of The Electrochemical Society **164**(7), A1679–A1687 (2017)
[24] Plett, G.L.: Battery management systems, Volume I: Battery modeling, vol. 1. Artech House (2015)
[25] Plett, G.L.: Battery management systems, Volume II: Equivalent-circuit methods, vol. 2. Artech House (2015)
[26] Rahimian, S.K., Rayman, S., White, R.E.: Extension of physics-based single particle model for higher charge–discharge rates. Journal of Power Sources **224**, 180–194 (2013)
[27] Reniers, J.M., Mulder, G., Howey, D.A.: Review and performance comparison of mechanical-chemical degradation models for lithium-ion batteries. Journal of The Electrochemical Society **166**(14), A3189–A3200 (2019)
[28] Santhanagopalan, S., Guo, Q., Ramadass, P., White, R.E.: Review of models for predicting the cycling performance of lithium ion batteries. Journal of Power Sources **156**(2), 620–628 (2006)
[29] Santhanagopalan, S., White, R.E.: Online estimation of the state of charge of a lithium ion cell. Journal of power sources **161**(2), 1346–1355 (2006)

[30] Sharma, A.K., Basu, S., Hariharan, K.S., Adiga, S.P., Kolake, S.M., Song, T., Sung, Y.: A closed form reduced order electrochemical model for lithium-ion cells. Journal of The Electrochemical Society **166**(6), A1197–A1210 (2019)
[31] Subramanian, V.R., Ritter, J.A., White, R.E.: Approximate solutions for galvanostatic discharge of spherical particles i. constant diffusion coefficient. Journal of The Electrochemical Society **148**(11), E444–E449 (2001)